Gas Processing Journal
Vol. 5, No. 2, 2017
http://gpj.ui.ac.ir
DOI: http://dx.doi.org/10.22108/gpj.2018.108384.1019

CFD Simulation of a Wetted-Wall Column for Natural Gas Sweetening Using DEA Solution

Samaneh Bayati [1], Ali Mohebbi [2*]

[1,2] Department of Chemical Engineering, Faculty of Engineering, Shahid Bahonar University of Kerman, Kerman, Iran

Article History
Received: 2017-12-04 Revised: 2018-05-31 Accepted: 2018-06-09

Abstract
Natural gas usually contains significant amounts of acid gases when it is extracted from underground reservoirs. Therefore, it must be treated by appropriate processes to remove these acidic components. In this study, the simultaneous absorption of carbon dioxide and hydrogen sulfide from natural gas into diethanol amine solution was simulated using CFD. Absorption process was performed in a wetted-wall column with counter-current gas-liquid flow. A two-dimensional simulation based on the volume of fluid model was used. To investigate the hydrodynamics of the flow in the column, distribution of the volume fraction of phases along the column, the formation of liquid film and velocity profiles were studied. To validate the results for predicting the liquid film thickness, the column was simulated at different flow rates of water and air in laminar flow regime. Simulation results for liquid film thickness were compared with experimental data. Then by considering the mass transfer from the gas phase to liquid phase based on Higbie's penetration theory, the concentration distribution of components in gas and liquid phases was calculated. The effect of temperature on absorption of CO_2 and H_2S was also studied. The comparison of simulation results with the experimental data for the outlet concentrations in the gas phase showed that there was a good agreement between them. The developed model can also be used in further studies to determine the effective parameters on simultaneous absorption of CO_2 and H_2S in a wetted-wall column. This helps to optimize the performance of the sweetening process in gas refineries.

Keywords
Natural gas sweetening; Carbon dioxide; Hydrogen sulfide; CFD; DEA

1. Introduction

Natural gas is the most important and the most common fossil fuels in the current age and future. In the world today, natural gas is widely used in household, industries and transportation. Since natural gas is located in deep underground reservoirs, it may contain several non-hydrocarbon components such as carbon dioxide and hydrogen sulfide so it is called sour gas. Gas sweetening is the separation of acid gases from sour gas. Acid gases in the sour gas are undesirable compounds, which cause several problems such as corrosion and environmental pollutions without any thermal value. Therefore, before using natural gas, acid gases should be removed by sweetening processes in the treatment units (Abdulrahman & Sebastine, 2013; Rahimpour, Saidi, Baniadam, & Parhoudeh, 2013). Due to the presence of impurities such as acid gases in natural gas and the problems caused by them, separation processes to remove these gases have always been an important issue. The increasing importance and application of natural gas as an energy source lead to challenges related to the design of separation and purification processes. The utilization of natural gas extracted from natural resources is limited because of high corrosion and environmental problems caused by acid gases. Gas sweetening is usually done in tray towers, packed towers, venturi and spray scrubbers, bubble columns and wetted wall columns (Baniadam, Fathikalajahi, & Rahimpour, 2009; Keshavarz, Fathikalajahi, & Ayatollahi, 2008). Wetted

* **Corresponding Author.**
Authors' Email Address:
[1] **S. Bayati** (bayati_samaneh@yahoo.com), [2] **A. Mohebbi** (amohebbi@uk.ac.ir.),

ISSN (Online): 2345-4172, **ISSN (Print):** 2322-3251

wall columns are important equipment in separation processes and are widely used in theoretical studies of mass transfer because of their simple structure, the specified interface of the two phases and possibility of controlling the process. Among different methods for removing $CO_2$and H_2S, chemical absorption using alkanolamine solutions have great applications.

Alkanolamines are widely used for acidic components removal from natural gas (Baniadam et al., 2009). Monoethanolamine (MEA), Diethanolamine (DEA), Diisopropanolamine (DIPA) and N-Methyldiethanolamine (MDEA) are the most commonly used amines for removal of CO_2 and H_2S (Mandal & Bandyopadhyay, 2006). MEA and DEA are widely used for simultaneous absorption of CO_2 and H_2S from sour gas and industrial gas streams but MDEA is often used for selective removal of H_2S from gas streams containing both CO_2 and H_2S (Mandal & Bandyopadhyay, 2005). Many efforts have been done in the field of natural gas sweetening and finding new ways to increase the efficiency of acid gases removal during the past years.

Yih and Sun (1986) worked on simultaneous absorption of CO_2 and H_2S using potassium carbonate and amine-promoted potassium carbonate solutions in a 183 cm long wetted wall column of outside diameter of 2.72 cm. The influences of gas and liquid flow rate, temperature, solvent concentration, promoter type and concentration on absorption rate, mass transfer coefficient and selectivity factor were studied. It was observed that DEA was a more effective promoter for absorption of CO_2 and H_2S.

Mandal and Bandyopadhyay (2005) studied the simultaneous absorption of CO_2 and H_2S into aqueous blends of 2-amino-2-methyl-1-propanol (AMP) and diethanolamine (DEA) in their theoretical and experimental investigations. The effects of contact time, amine concentration and temperature on the absorption rate and the selectivity were investigated by absorption experiments in a wetted wall column at atmospheric pressure with a constant feed gas ratio. The diffusion–reaction processes for CO_2 and H_2S mass transfer in blended amines were modelled according to Higbie's penetration theory with the assumption of reversible reactions. It was observed that the blended amine solvent was an efficient mixture solvent for simultaneous absorption of CO_2 and H_2S and by varying the relative amounts of AMP and DEA, the solvent selectivity for absorption of CO_2 and H_2S can be changed.

Mandal and Bandyopadhyay (2006) also studied the simultaneous absorption of CO_2 and H_2S into aqueous blends of DEA and MDEA in their theoretical and experimental investigations. The effect of contact time, temperature and amine concentration on the rate of absorption and the selectivity were investigated by absorption experiments in a wetted wall column at atmospheric pressure and constant feed gas ratio. The diffusion–reaction processes for CO_2 and H_2S mass transfer in blended amines were modelled according to Higbie's penetration theory with the assumption that all reactions are reversible. Model results based on the kinetics-equilibrium-mass transfer coupled model were found to be in good agreement with the experimental data for absorption rates of CO_2 and H_2S into (MDEA + DEA + H2O).

Baniadam et al. (2007) developed a 2D mathematical model for acid gases (i.e. CO_2 and H_2S) removal in a commercial sieve tray column using MDEA. The velocity profile in the liquid phase in both radial and axial directions was calculated using computational fluid dynamics. Mass and energy equations also were derived and numerically solved in order to define the concentration and temperature profiles in radial and axial directions. The model was based on two film theory.

Xu, Paschke, Repke, Yuan, & Wozny (2009) studied the mechanism of absorption and momentum transfer in a laminar, counter current gas and liquid film flow on a plate in a three-dimensional model using computational fluid dynamics. The volume of fluid (VOF) model was used to investigate the hydrodynamics and mass transfer between gas and liquid phases based on penetration theory. Experiments and simulations were done for a system of propane and toluene. The irregular surface of the liquid film, velocity profiles in gas and liquid phases, concentration profiles and output concentrations were studied. There was a good agreement between simulation results and experimental data.

Rezakazemi et al. (2010) studied the chemical absorption of CO_2 and H_2S in a hollow fibre membrane contactor (HFMC) theoretically and experimentally. A 2D mathematical model was developed for simultaneous absorption of CO_2 and H_2S in a HFMC using MDEA solution. The radial and axial diffusion were considered in that model. The effects of convection and chemical

reactions were also considered in both the shell and tube. Computational fluid dynamics (CFD) was used to solve the equations of continuity and momentum. The experimental data confirmed the model predictions and good agreement was observed between simulation results and experimental data for different values of gas and liquid velocity. The simulation results showed that H_2S removal using MDEA solution was very high and H_2S was almost completely removed. Their results showed that the membrane used for removal of small amounts of H_2S was very effective in high gas to liquid ratios. The model was able to predict the absorption performance of CO_2 and H_2S in the HFMC.

In order to screen different amine solvents for CO_2 capture, Chen, Closmann, and Rochelle (2011) used a wetted-wall column to measure CO_2 equilibrium partial pressure and absorption/ desorption rates at various CO_2 loading from 40 to 100℃. The heat of absorption, CO_2 capacity and liquid film mass transfer coefficients were also determined in this study. The results showed that primary amines used in this research (DGA, MAPA and MEA) had low CO_2 capacity, low absorption rates and high heat of absorption. AMP had a high CO_2 capacity but suffered from low absorption rate. MDEA blended with PZ showed high CO_2 capacity and absorption rate with a lower heat of absorption in comparison to primary amines.

Rahimpur et al. (2013) developed a mathematical model based on computational fluid dynamics for absorption of acid gases into amine solution in a structured packing with corrugated sheets. 2D mass and energy equations with chemical reactions between acid gases and amine solution were derived for cylindrical coordinate since corrugated plates placed in a way that channels were created along the bed. The temperature and concentration profiles were obtained over the bed in the gas and liquid by solving the governing equations based on mass and energy conservation equations.

Rodriguez-Flores, Mello, Salvagnini, and de Paiva (2013) studied CO_2 absorption into MEA, AMP and their respective blend to evaluate the absorption process and determine a design parameter for a single-amine absorption system. A wetted- wall column with a film promoter, a thin stainless steel woven, was used for experimental tests which were carried out in counter-current flow at 298 K, atmospheric pressure, a constant gas load (10% CO_2) and three different liquid loads. It was concluded that the interfacial area was influenced by increasing the liquid load which means an increase in the effective interfacial area between liquid and gas phase. The values of K_Ga related to MEA and the blend based on it were higher in comparison to AMP and the results showed that K_Ga value for MEA: AMP mixtures increased by increasing the MEA proportion in the blend.

Hosseini, Alizadeh, Fatehifar, and Alizadehdakhel (2014) studied the chemical absorption of CO_2 into the monoethanolamine solution in a wetted wire column consisting of one wire. The two-phase flow, mass transfer and chemical reaction were simulated using computational fluid dynamics method with applying volume of fluid model. The simulation results were in good agreement with experimental data. Their simulation results showed that by increasing the gas and liquid flow rates, the diameter and intervals of liquid beads increased. The beads velocity also increased by increasing the liquid flow rate and decreasing the mass fraction of MEA in the liquid phase and mass transfer resistance in the liquid phase reduced by formation of the beads. Finally, they concluded that their model was able to predict the effect of physical and operating parameters on the investigated chemical absorption process.

Taheri, Mohebbi, Hashemipour, and Rashidi (2016) employed a wetted-wall column to study the simultaneous removal of CO_2 and H_2S from natural gas using a nanofluid containing SiO_2 and Al_2O_3 nanoparticles and nanoporous graphene in Diethanolamine. The effects of concentration and particle types on absorption of CO_2 and H_2S were studied. The experiments were done at 298 K and with two different inlet gas compositions. The results showed that SiO_2-DEA nanofluid had deteriorating effects on H_2S removal while Al_2O_3 -DEA improved H_2S absorption. It was also observed that CO_2 absorption rate was enhanced with both Al_2O_3 –DEA and SiO_2-DEA nanofluids but SiO_2 was found to be a more effective candidate for CO_2 absorption. It was also found that the presence of naoporous graphene in DEA solution had a significant effect on absorption of CO_2 and H_2S in comparison to DEA.

Karlsson and Svensson (2017) investigated CO_2 absorption rate using a wetted- wall column with two different solvents, MEA and mixture of AMP in the NMP. Experiments were carried out for various concentrations of amine solutions and the results showed a higher flux and higher liquid side mass

transfer of CO_2 for the mixture of AMP in NMP compared to aqueous MEA.

Lillia, Bonalumi, Fosbøl, Thomsen, and Valenti (2018) studied the absorption of CO_2 into NH_3 using a wetted- wall column in order to investigate the effect of solvent condition on the rate of reaction. The experimental tests were done at different temperatures, various NH_3 concentrations and different CO_2 loadings. They presented the raw data and also the final value of the overall mass transfer coefficient as a result of the raw data treatment.

Wang, Xu, Lai, and Sun (2018) developed a multiphase computational fluid dynamics (CFD) model in order to determine the CO_2 mass transfer coefficient in solvent-based CO_2 capture using a wetted- wall column. A volume of fluid model was used to model the hydrodynamics and the diffusive and reactive mass transfer between the two phases was modelled by applying a one-fluid formulation. The results for the mass transfer coefficients were compared with the standard two-film theory (STFT).

The aim of this study was the simulation of a counter-current wetted-wall column for simultaneous removal of CO_2 and H_2S from natural gas using computational fluid dynamics. The solvent of absorption process was DEA. A 2D simulation based on the volume of fluid (VOF) model was developed. After studying the hydrodynamics of the column, mole fractions of CO_2 and H_2S were calculated in the gas output considering mass transfer from the gas phase to the liquid phase (i.e. absorption of acid gases into the amine solution) and simulation results were compared with the experimental data.

2. Simulation Procedure

2.1. Geometry

The structure of the wetted wall column used in this simulation is based on the experimental set up in the Sarkhoon and Qeshm gas Refinery Company for CO_2 and H_2S removal from natural gas. The wetted wall column is made up of two concentric tubes. The inner one is 8 cm long stainless steel wetted- wall tube with an outer diameter of 0.635 cm and thickness of 0.1 cm. The outer tube is 8.5 cm long pyrex tube with an inner diameter of 2.54 cm. Due to the symmetrical geometry of the column, a two-dimensional axisymmetric model was selected for simulation of the two-phase flow in the column. Dimensions of the column are shown in Fig. 1.

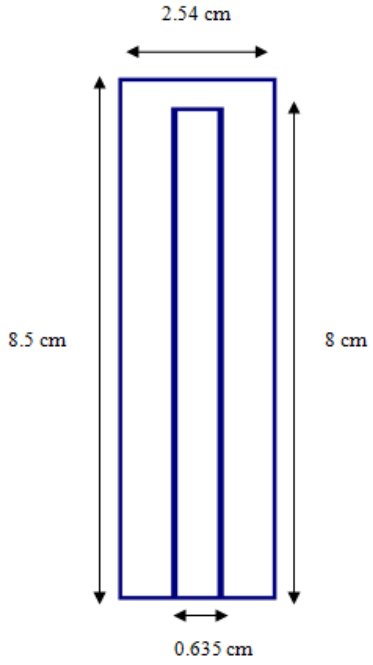

Figure 1. Dimensions of the wetted-wall column

2.2. Governing Equations

2.2.1. Conservation Equations

Conservation equations are used for obtaining the main equations of the laminar fluid flow. For all kind of flows, FLUENT solves the conservation equations of mass and momentum. By writing the mass and momentum balances around a small element of fluid, Navier-Stokes and continuity equations are derived. The velocity and pressure distribution of the fluid are obtained from solving these equations (Fluent 6.3.26 users guide, 2006; Hosseini, 2013).

The general form of the continuity equation is shown in Eq. (1) (Fluent 6.3.26 users guide, 2006):

$$\frac{\partial \rho}{\partial t} + \nabla . (\rho \vec{v}) = 0 \qquad (1)$$

where ρ and $\vec{v}$ are density and the velocity vector respectively.

The conservation equation of momentum in the inertial coordinate system is as follows (Fluent 6.3.26 users guide, 2006):

$$\frac{\partial}{\partial t}(\rho \vec{v}) + \nabla . (\rho \vec{v} \vec{v}) = -\nabla p + \nabla . (\bar{\bar{\tau}}) + \rho \vec{g} + \vec{F} \qquad (2)$$

Here p is the static pressure, $\bar{\bar{\tau}}$ is the stress tensor, $\rho \vec{g}$ and $\vec{F}$ are the gravitational and external body forces respectively. By substituting the equation of stress tensor in

Eq. (2), the momentum equation is derived as follows (Fluent 6.3.26 users guide, 2006):

$$\frac{\partial}{\partial t}(\rho\vec{v}) + \nabla.(\rho\vec{v}\vec{v}) = -\nabla p + \nabla.\mu(\nabla\vec{v} + \nabla\vec{v}^T) + \rho\vec{g} + \vec{F} \quad (3)$$

2.2.2. Volume Fraction Equations

In a two- phase flow in which the two fluids are immiscible, VOF model is used to track the interface betweenthe two phases. In this model, the volume fraction of each phase is defined as a variable (Hosseini et al., 2014). The total volume fraction of phases is one in each control volume. The equation of volume fraction for liquid phase is shown in Eq. (4) (Ho et al., 2011).

$$\frac{\partial}{\partial t}(\alpha_l\rho_l) + \nabla.(\alpha_l\rho_l\vec{v}_l) = 0 \quad (4)$$

This equation is derived from the conservation of mass in the liquid phase. Since the sum of volume fraction of phases is equal to 1, the gas volume fraction (α_g) is calculated from Eq. (5) (Ho et al., 2011).

$$\alpha_l + \alpha_g = 1 \quad (5)$$

The volume averaged density and viscosity are estimated using the following equations (Ho et al., 2011).

$$\rho = \alpha_l\rho_l + (1-\alpha_l)\rho_g \quad (6)$$

$$\mu = \alpha_l\mu_l + (1-\alpha_l)\mu_g \quad (7)$$

In Fluent software, the effect of surface tension along the interface of phases is considered by using the continuum surface force (CSF) model. In this model, by applying the surface tension to the VOF calculations, a source term appears in the momentum equation. The source term is as follows (Hosseini et al., 2014):

$$\vec{F} = \sigma\frac{\rho K\alpha_l}{\frac{1}{2}(\rho_l+\rho_g)} \quad (8)$$

where K is the interface curvature and is computed from the gradients of the unit normal $\hat{n}$ at the interface (Hosseini, 2013; Hosseini et al., 2014).

$$K = \nabla.\hat{n} \quad (9)$$

here $\hat{n}$ is as follows:

$$\hat{n} = \frac{\nabla\alpha}{|\nabla\alpha|} \quad (10)$$

In Fluent, the effect of contact angel between the wall and the fluid is applied by a boundary condition. Near the wall, the contact angle is defined as a measure of adhesion. This boundary condition is applied to the cells near the wall and adjusts the curvature of the interface in these cells. θ_c is the contact angel between the fluid and the wall, so the surface normal vector in the cell next to the wall is calculated from Eq. (11).

$$\hat{n} = \hat{n}_w cos\theta_c + \hat{t}_w sin\theta_c \quad (11)$$

where $\hat{n}_w$ and $\hat{t}_w$ are the unit normal and tangent vectors to the wall (Ho et al., 2011). So, the defined surface curvature for cells is used for the surface tension calculations (Chen et al., 2011).

2.2.3. Mass Transfer

The fluid flow in the wetted wall column for simultaneous absorption of carbon dioxide and hydrogen sulfide is along with mass transfer between two phases and also chemical reaction. Species transport equation is derived by solving the conservation equation of chemical species in the multiphase flows. The equation of species transport is as follows (Fluent 6.3.26 users guide, 2006):

$$\frac{\partial}{\partial t}(\rho^q\alpha^qY_i^q) + \nabla.(\rho^q\alpha^q\vec{v}^qY_i^q) = -\nabla.\alpha^q\vec{J}_i^q + \alpha^qR_i^q + \sum_{p=1}^{n}(\dot{m}_{p^jq^i} - \dot{m}_{q^ip^j}) \quad (12)$$

where α^q is the volume fraction of phase q, Y_i^q is the mass fraction of component i in the phase q, $\vec{J}_i^q$ is the vector of mass transfer flux for component i in the phase q, R_i^q is the production rate of component i by chemical reaction in the phase q and $\dot{m}_{q^ip^j}$ is the mass transfer rate between components i and j from phase q to the phase p.

2.2.4. Mass Transfer Equation at the Interface

Mass transfer rate at the gas-liquid interface is calculated from the equation based on the two-film theory (Hosseini et al., 2014).

$$\dot{m}_{lg,n} = Ek_la_eM^nC_l(x_n^i - x_n^b) = k_ga_eM^nC_g(y_n^b - y_n^i) \quad (13)$$

where x_n^i and y_n^i are the mole fraction of component n at the interface of liquid and gas phases, x_n^b and y_n^b are the mole fraction of component n in the bulk liquid and gas phases, a_e is the specific area, M^n is the molecular weight of component n, C is the total concentration of each phase, k_l and k_g are the

mass transfer coefficients in liquid phase and gas phase respectively and E is the enhancement factor for considering the effect of chemical reaction. Using the two- film theory and the assumption of equilibrium at the gas- liquid interface, the relationship between x_n^i and y_n^i is obtained by Henry's law.

$$C_l x_n^i He = p y_n^i \quad (14)$$

in the equation (14), the unit of Henry's constant is $\frac{kPa.m^3}{kmol}$.

Using the penetration theory, mass transfer coefficients in gas and liquid phases are calculated as follows (Hosseini, 2013):

$$k_g = 2\sqrt{\frac{D_{n,g}}{\pi \tau_g}} \quad (15)$$

$$k_l = 2\sqrt{\frac{D_{n,l}}{\pi \tau_l}} \quad (16)$$

The contact time at the interface of the two phases is the same and is calculated as follows (Hosseini, 2013):

$$\tau_g = \tau_l = \frac{L_i}{w_x^i} \quad (17)$$

where L_i is the length of each cell along the flow for numerical simulation and w_x^i is the interface velocity along the flow.

Because of chemical reaction between CO_2 and amines, the molecular diffusion coefficient of CO_2 cannot be measured directly. So, the N_2O analogy can be used to estimate the diffusion coefficient of carbon dioxide into amine solutions. Based on this analogy, due to the similarities between CO_2 and N_2O molecular structures, diffusion coefficient of CO_2 into amine solutions is proportional to the diffusion coefficient of N_2O into amine solutions. This analogy is shown by Eq. (18).

$$D_{CO_{2,m}} = D_{N_2O,m}\left(\frac{D_{CO_{2,w}}}{D_{N_2O,w}}\right) \quad (18)$$

Where $D_{CO_{2,w}}$ and $D_{N_2O,w}$ are the diffusion coefficients of CO_2 and N_2O into water and are calculated as follows:

$$D_{CO_{2,w}} = 2.35 \times 10^{-6}\, exp\left(-\frac{2119}{T}\right) \quad (19)$$

$$D_{N_2O,w} = 5.07 \times 10^{-6}\, exp\left(-\frac{2371}{T}\right) \quad (20)$$

and Eq. (21) is used to calculate the diffusion coefficient of N_2O into DEA solution (Ko, Tsai, Lin, Wang, & Li, 2001).

$$D_{N_2O,m} = (5.07 \times 10^{-6} + 2.17 \times 10^{-6} \times C_{DEA} + 2.29 \times 10^{-6} \times {C_{DEA}}^2) \times exp\left(\frac{-2371 - 2.92 \times 10^2 \times C_{DEA}}{T}\right) \quad (21)$$

where C_{DEA} is the concentration of DEA solution in terms of $kmol/m^3$.

The diffusion coefficient of H_2S into amine solution is calculated by the modified equation of Stokes- Einstein as follows (Hosseini, 2013):

$$D_{H_2S,m} = D_{H_2S,w}\left(\frac{T}{T_w}\right)\left(\frac{\mu_w}{\mu}\right)^{0.6} \quad (22)$$

where μ_w is the viscosity of water and $D_{H_2S,w}$ is the diffusion coefficient of H_2S into water at T_w.

The N_2O analogy is also used to determine Henry's constant of CO_2 for absorption of it into DEA solution. The Eq. (23) shows this analogy (Penttilä, Dell'Era, Uusi-Kyyny, & Alopaeus, 2011).

$$H_{CO_{2,m}} = H_{N_2O,m}\left(\frac{H_{CO_{2,w}}}{H_{N_2O,w}}\right) \quad (23)$$

The Henry's constants for dissolution of CO_2 and N_2O in water are defined as follows (Penttilä et al., 2011):

$$H_{CO_{2,w}} = exp\left(145.369 - \frac{8172.355}{T} - 19.303 ln T\right) \quad (24)$$

$$H_{N_2O,w} = exp\left(158.245 - \frac{9048.596}{T} - 20.860 ln T - 0.00252T\right) \quad (25)$$

The Henry's constant for dissolution of N_2O into pure DEA is calculated by the Eq. (26) (Penttilä et al., 2011).

$$H_{N_2O,DEA} = -11958 + 50.478T \quad (26)$$

Equation (27) is used to calculate Henry's constant for dissolution of N_2O in DEA solution (Penttilä et al., 2011).

$$H_{N_2O,12} = \sum_{i=1}^{2} H_{N_2O,i} x_i + 4899600.015[x_1 x_2]^2 \left[1 - \frac{T}{362.079}\right] exp[-15.809 x_2] \quad (27)$$

here x_i is the mole fraction of component i in the solvent. 1 refers to the water and 2 refers to the DEA. In the above equations, the Henry's constant is in terms of $\frac{Pa.m^3}{mol}$ and temperature is in term of K.

The Henry's constant for dissolution of H_2S in water is calculated from the following equation (Carey, Hermes, & Rochelle, 1991):

$$H_{H_2S,w} = \frac{\exp(342.595 + 0.0595651 \times T - 55.0551 lnT - \frac{13236.8}{T})}{\rho_w} \quad (28)$$

where $H_{H_2S,w}$ is in terms of $\frac{atm.m^3}{mole}$.

When two gases are simultaneously absorbed in a solution containing a component which can react with both of the gases, the absorption rate of each gas would be affected by the other one. The reaction of H_2S with primary and secondary amines can be considered as an instantaneous reaction. An instantaneous reaction is limited by diffusion. Since the reaction is very fast, the reactant and the absorbed gas in the liquid phase cannot simultaneously exist in the same area of the liquid. The reaction of CO_2 with primary and secondary amines is very slower than the reaction of H_2S and often can be considered the second order. In this research, the simultaneous absorption of two gases into the liquid containing a component that reacts with both of the gases is simulated based on Higbie's penetration theory. The reaction of H_2S with DEA is instantaneous and the reaction of CO_2 with DEA is considered second order (Haimour & Sandall, 1983).

Because of chemical reaction in the liquid phase, R_i in Eq. (12) should be substituted with the kinetics of reaction. Equation (29) gives the mechanism of reaction between H_2S and DEA. Since this reaction is so fast, it can be considered as an instantaneous reaction. The mechanism of reaction between CO_2 and DEA is also given by Eq. (30) (Versteeg, Van Dijck, Van Swaaij, 1996).

$$R'R'NH + H_2S \leftrightarrow R'R'NH_2^+ + HS^- \quad (29)$$

$$R'R'NH + CO_2 \leftrightarrow R'R'NCOO^- + H^+ \quad (30)$$

here R′R′NH is DEA and $R' = CH_2CH_2OH$. Equation (31) shows the rate of the reaction between CO_2 and DEA using the reaction constant developed by Blanc and Demarais (Versteeg et al., 1981).

$$R_{CO_2} = 2.81 \times 10^7 exp(-\frac{5237}{T})[CO_2][DEA] \quad (31)$$

in which T is in term of K and concentrations are in terms of $\frac{mol}{m^3}$.

2.3. Solution Method

Due to the dynamic nature of the two-phase flow, unsteady state calculations were chosen for the solution of the equations with a time step of 10^{-5}s and the residual amount of the parameters was considered 0.001. The SIMPLE algorithm was used for pressure-velocity coupling calculations. The PRESTO! method was selected for discretizationof the pressure equation and a second order upwind calculation method was applied for discretization of momentum, volume fraction and species equations. The equations of mass transfer rate between two phases were defined using the user-defined function (UDF).

2.3.1. Initial and Boundary Conditions

Uniform velocity inlet and atmospheric pressure outlet were used as boundary conditions for inlet and outlet of the phases respectively. At the walls of the column, no-slip boundary condition was applied. At time zero, gas and liquid velocity magnitudes and volume fraction of liquid phase were set to zero as initial conditions.

Table 1 shows the compositions, volume flow rates and inlet velocities for both gas and liquid phases.

Table 1. Compositions, volume flow rates and inlet velocities for gas and liquid phases

Phase	Composition	Volume flow rate ($^{L}/_{min}$)	Inlet velocity ($^{m}/_{s}$)
Liquid	10 % wt DEA 90 %wt water	0.055	0.0617
Gas	23 ppm H_2S 1 %mol CO_2 CH_4	0.5592	0.01962

3. Results and Discussion

In this section, the results of CFD simulation for VOF profile and liquid film formation with time, pressure, velocity and concentration profiles are presented. Simulation results for mole fractions of CO_2 and H_2S in output gas are compared with experimental data. Then the concentration distribution in gas and liquid phases and the effect of temperature on absorption process are investigated.

Figure 2 shows the geometry generated in Gambit software for liquid film formation. After the complete formation of the liquid film, since the effective length for absorption process is x=0 to x=8 cm, the geometry shown in Fig. 3 was used for mass transfer simulation.

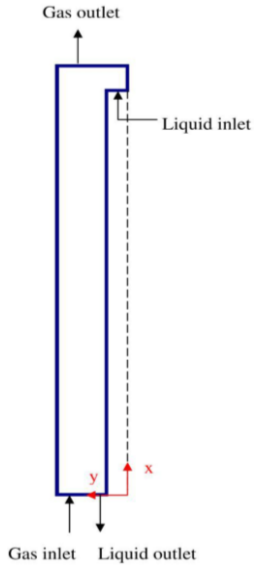

Figure 2. The generated geometry in Gambit software for simulation of liquid film formation

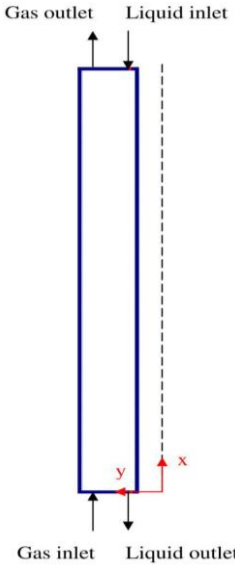

Figure 3. The generated geometry in Gambit software for simulation of mass transfer process

In order to reduce the calculations time and also less precision required in the gas phase, smaller and larger grid sizes were used for liquid and gas regions respectively. The grid independency was checked by using three different mesh sizes with a total number of 116850, 121000 and 142750 cells. The results of these three cases were close together for the average thickness of the liquid film. Therefore the grid with 121000 numbers of cells was selected as the suitable grid.

3.1. Validation of Simulation Results for Liquid Film Thickness

In order to validate the simulation results for liquid film thickness, as respects the liquid film thickness for 10% DEA solution has not been measured experimentally, the column is simulated for different flow rates of water-air flows in laminar flow regime. The results of these simulations for the film thickness are compared with the experimental data published by Yih and Hsu (1985) and also Zhou, Gambaryan-Roisman, and Stephan (2009) in laminar flow regime. Table 2 gives the results of these comparisons. As it is observed, by increasing the Reynolds number, the average film thickness increases and there is a good agreement between simulation results and the experimental data. So it is concluded that the developed model can determine the liquid film thickness in laminar flow regime and does not need to guess an initial value for film thickness unlike similar works previously done.

3.2. VOF Profile

To determine the volume fraction of each phase, VOF equation with mass conservation (continuity) and conservation of momentum (Navier-Stokes) equations were solved. Figure 4 shows the formation of the liquid film with time. In this figure, red colour refers to the presence of DEA solution and the dark blue refers to the presence of natural gas (CH_4+CO_2+H_2S). As it can be seen, after the liquid overflows, a thin film streams down on the wall and finally exits the column. It takes about 48 seconds to form a stable liquid film.

Table 2. Comparison of simulation results and experimental data for liquid film thickness in two different Reynolds numbers of liquid

Re_l	$\delta_{simulation}$ (mm)	$\delta_{experimental}$ (mm) (Yih & Hsu, 1985)	$\delta_{experimental}$ (mm) (Zhou et al., 2009)
500	0.2850	0.2928	0.300
600	0.3288	0.3149	0.320

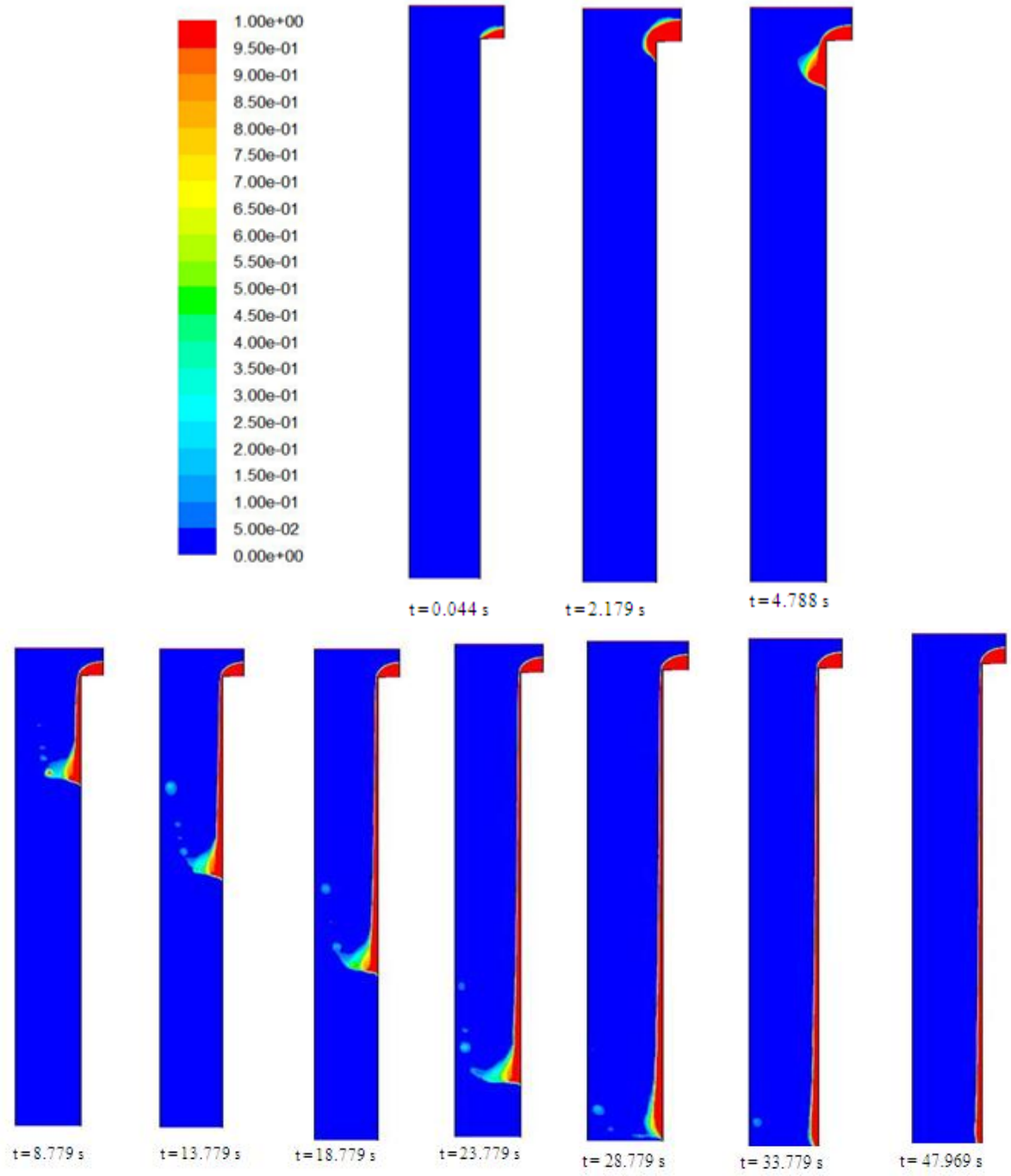

Figure 4. Contours of liquid volume fraction for aqueous DEA solution (10-wt% DEA) with the passage of tim

3.3. Velocity Profile

Obtaining the correct distribution of velocity is very important in order to simulate the counter current gas-liquid flow in the column. The simulation results for velocity magnitudes are shown in Figs. 5 and 6. As one can see, the velocity magnitude is zero on the wall due to applying a no-slip condition on this wall.

The profile of velocity magnitude at x= 4 cm is clearly shown in Fig. 6. As can be seen, the velocity magnitude is zero on the walls (r= 0.3175 cm and r= 1.27 cm) due to the no-slip condition. Because of the counter current gas-liquid flow, the mixture velocity tends to zero at r=0.64 cm.

Figure 7 shows the axial velocity contour so that the negative values refer to the liquid film flow in the opposite direction of gas flow. The profile of axial velocity at x= 4 cm is shown in Fig. 8. The gas-liquid counter current flow is clearly shown by negative values for downward liquid flow and positive values for upward gas flow in the column.

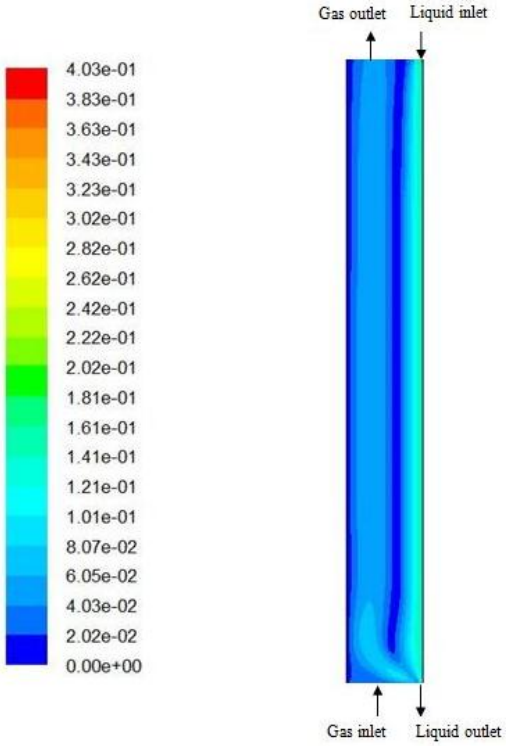

Figure 5. Contour of velocity magnitude for counter current gas-liquid flow in the wetted-wall column

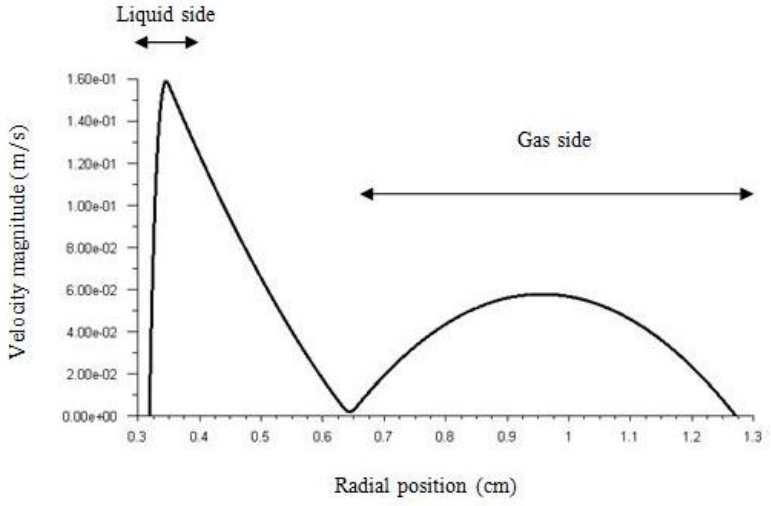

Figure 6. Profile of velocity magnitude (m/s) at x=4 cm

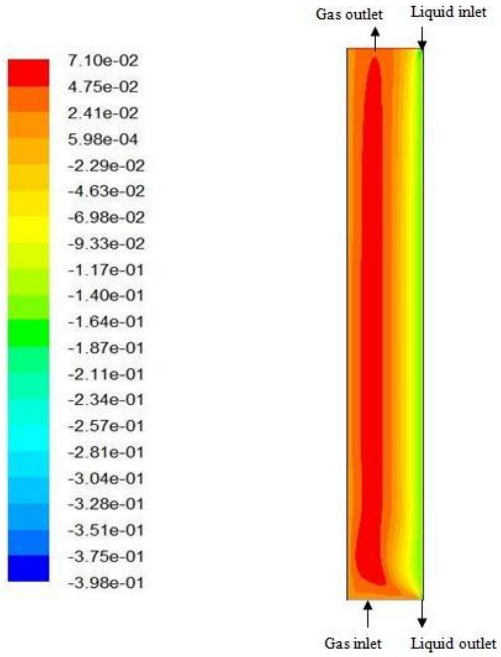

Figure 7. Axial velocity contour for counter current gas-liquid flow in the wetted-wall column

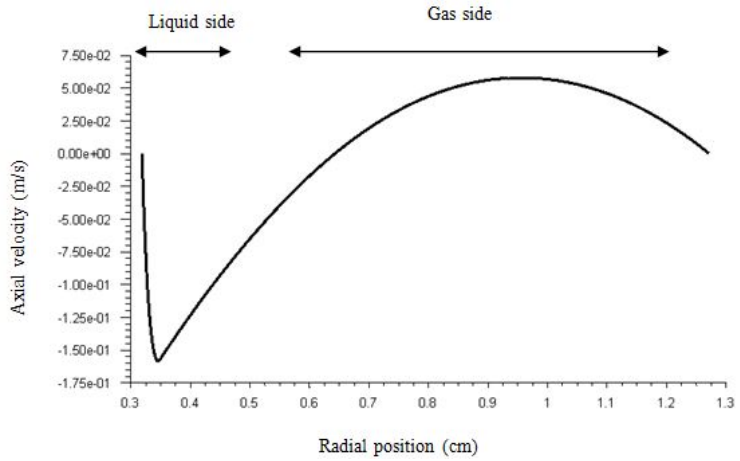

Figure 8. Profile of axial velocity (m/s) at x=4 cm

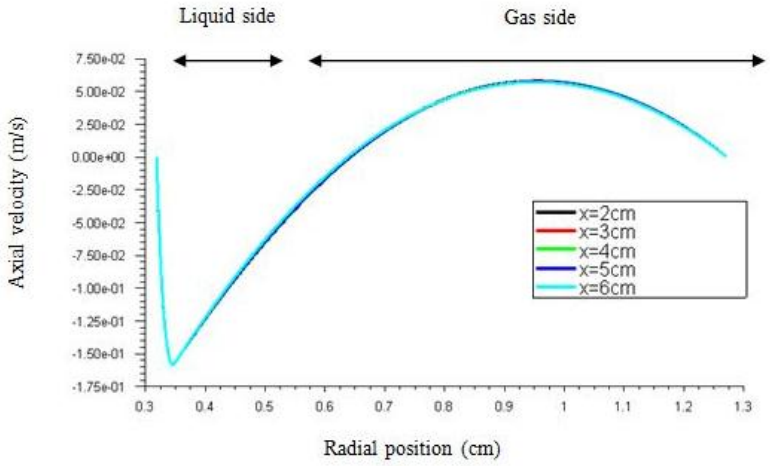

Figure 9. Comparison of axial velocity profiles in different heights of the column

In Fig. 9 axial velocity profiles in different heights of the column are compared together. As can be seen, the velocity profiles are completely coincident so that both liquid and gas flow in the column can be considered fully developed after x= 2 cm.

In Fig. 10 the counter-current flow of gas and liquid is clearly shown by using the vector form of axial velocity. As can be seen the liquid moves downward and the gas flow direction is upward.

3.4. Validation of the Simulation Results

In order to validate the applied model, simulation results for outlet concentrations of acid gases were compared with experimental data obtained in Sarkhoon and Qeshm gas refinery laboratory at 25, 30 and 35℃. Tables 3 and 4 show a good agreement between the simulation results and the experimental data. As the simulation results show, CO_2 and H_2S output mole fractions increased as the temperature increased. When the temperature increased from 25 ℃ to 30 ℃, CO_2 output mole fraction rose from 0.00701 to 0.00736 which is 4.99 % increase and H_2S output mole fraction increased from 6.04 ppm to 6.61 ppm which showed a rise of 9.44 %. At 35 ℃, CO_2 and H_2S output mole fractions increased 0.68 % and 11.8 % respectively toward 30 ℃. So, it can be concluded that H_2S was more sensitive to temperature changes.

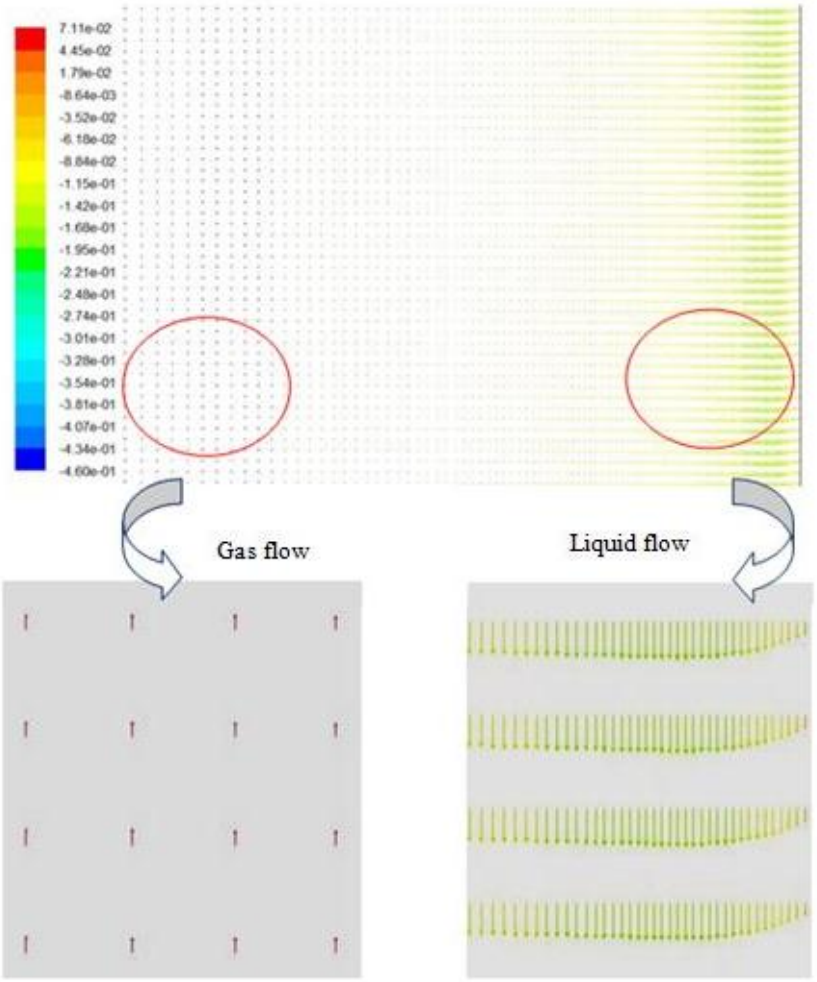

Figure 10. Vector form of the axial velocity (m/s) for counter current gas-liquid flow

Table 3. Comparison of simulation results and experimental data for CO_2 mole fraction in the column gas outlet

Temperature (℃)	Mole fraction of CO_2 in the gas outlet		Error (%)
	Simulation results	Experimental data	
25	0.00701	0.0075	6.5
30	0.00736	.0071	3.7
35	0.00741	0.0073	1.5

Table 4. Comparison of simulation results and experimental data for H_2S mole fraction in the column gas outlet

Temperature (℃)	Mole fraction of H_2S in the gas outlet (ppm)		Error (%)
	Simulation Results	Experimental data	
25	6.04	6	0.7
30	6.61	7	5.6
35	7.39	7	5.6

For obtaining the concentration distribution in the column, the species transport equations were solved with other equations simultaneously. The UDF was also applied for considering the mass transfer between two phases.

Mole fraction changes for CO_2 and H_2S in the gas phase are shown in Figs. 11 and 12 respectively. As expected, with the upward flow of the gas, the acid component mole fractions are decreased and in the upper part of the column due to the gas contact with fresh amine, more changes are observed for CO_2 and H_2S concentrations. As the solvent goes downward, the amount of absorbed acid gases is increased. Thus, fewer changes are observed in the acid gas concentrations in the lower part of the column.

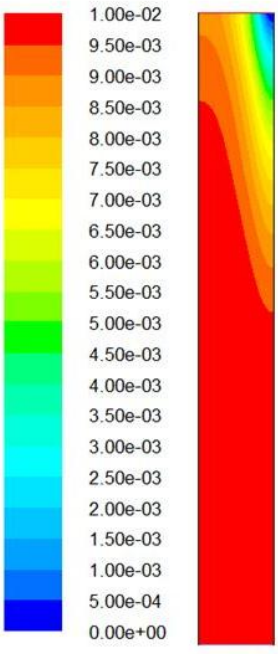

Figure 11. Contour of CO_2 mole fraction in the gas phase

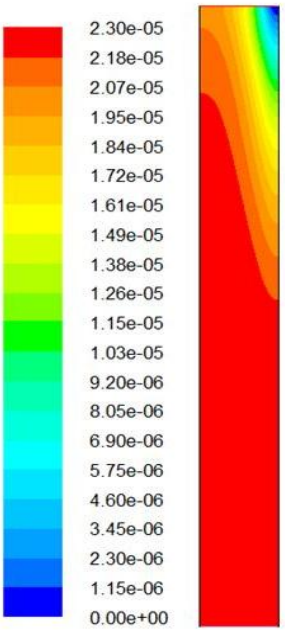

Figure 12. Contour of H_2S mole fraction in the gas phase

Figure 13 shows the changes of CO_2 mole fraction in radial direction at three different sections $x = 2$ cm, $x = 5$ cm and $x = 7$cm. As one can see, the mole fraction of CO_2 in the bulk gas is more than the gas interface and at the liquid interface is more than the CO_2 mole fraction in the bulk liquid. In the upper sections of the column, more concentration changes are observed in the gas phase due to the gas contact with fresh amine solution. Figure 14 compares the changes of radial CO_2 concentration profiles in the gas phase at different sections of the column. As it is shown, in the lower part of the column where the gas has just entered the column (x=2 cm), CO_2 concentration in the gas is high but with upward flow and absorption of CO_2 in the solvent, CO_2 concentration in the gas phase decreases in the upper part of the column (x=7 cm).

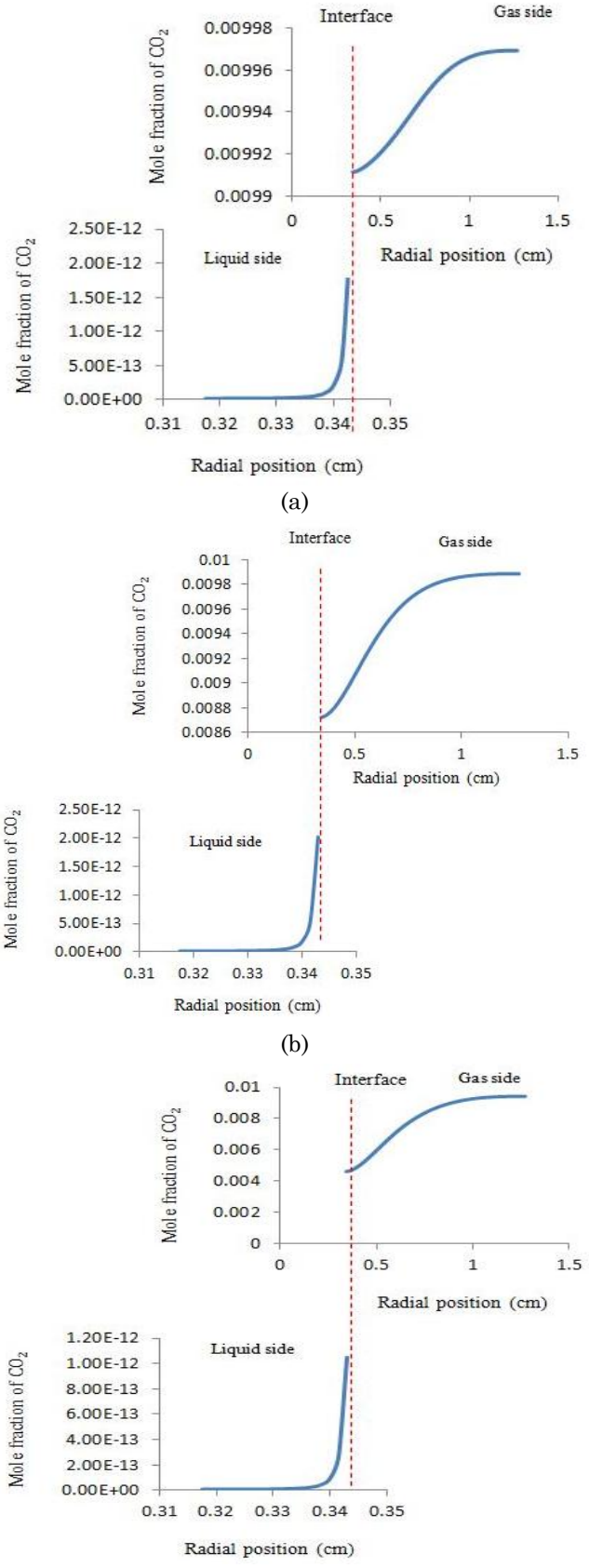

Figure 13. CO_2 mole fraction profiles at three different sections of the column (a) x=2cm (**b**) x=5cm (**c**) x=7cm

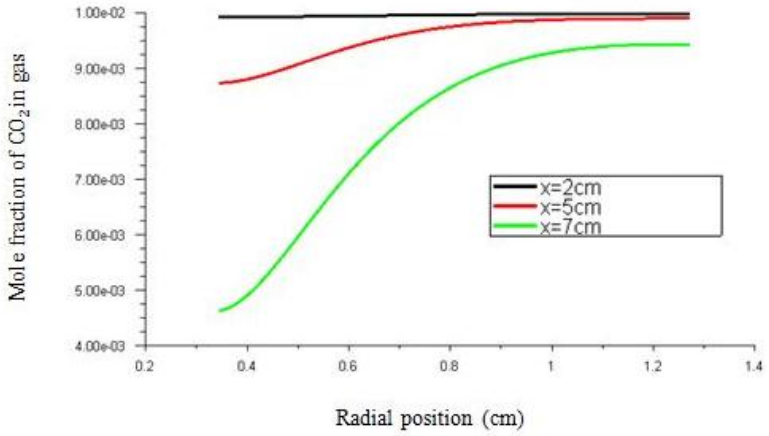

Figure 14. Comparison of CO_2 mole fraction profiles in the gas phase at different sections of the column

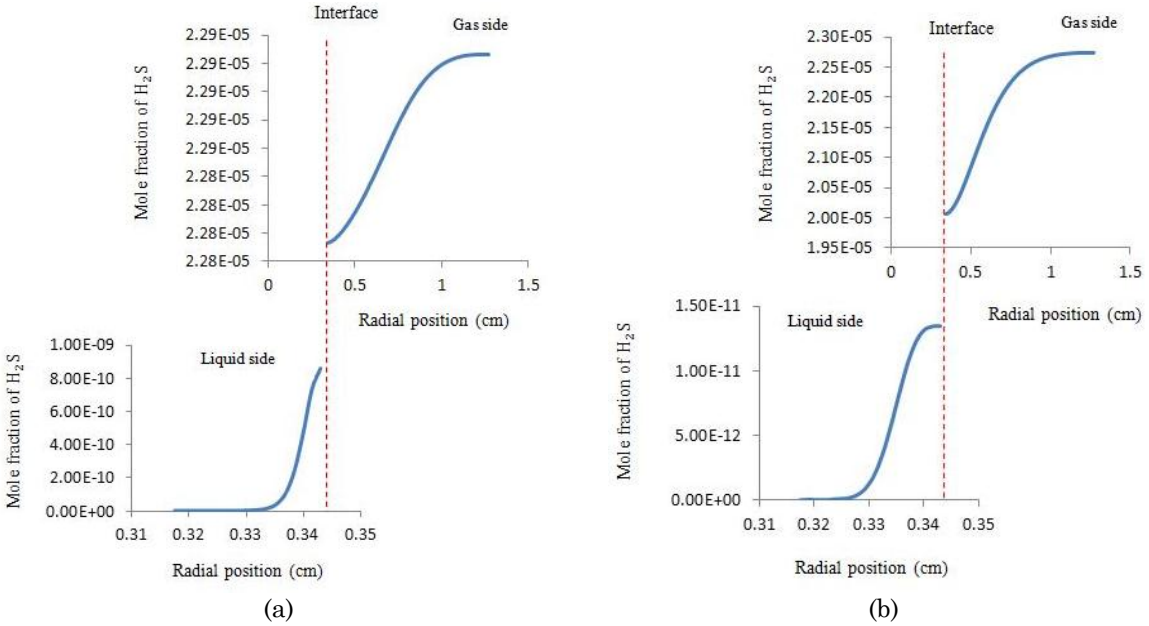

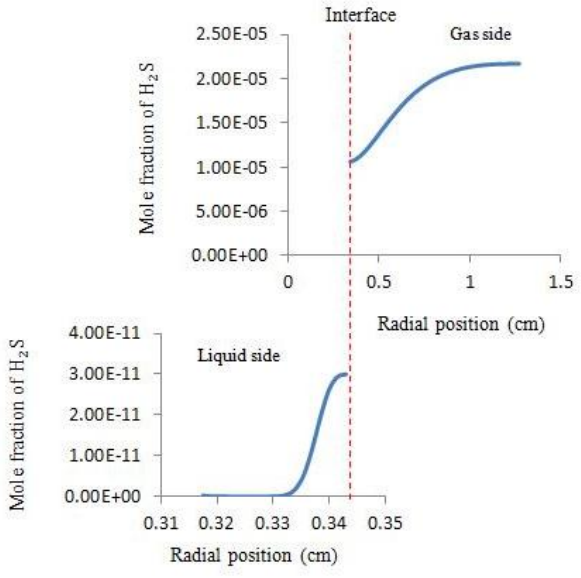

Figure 15. H_2S mole fraction profiles at three different sections of the column (a) x=2cm (**b)** x=5cm (**c)** x=7cm

Figures 15 and 16 also show H_2S concentration profiles. The changes of H_2S mole fraction in both gas and liquid phases at different heights of the column are shown in Fig. 15. As it is shown in Fig. 16, the mole fraction of H_2S in the gas phase decreases with upward flow and absorption of H_2S in the solvent. Figure 16 shows the changes of H_2S concentration profiles in the gas phase at different heights clearly. As the gas flows upward through the column, H_2S is absorbed in the amine solution, so more changes are observed in H_2S concentration in the gas phase at upper parts of the column.

When CO_2 is transferred from the gas to the liquid phase, it reacts with DEA in the solution and is consumed. Figure 17 shows the reaction rate in the liquid phase. As can be seen, CO_2 in the liquid phase is consumed according to a second-order reaction at the liquid interface and the reaction only occurs at the interface.

In a gas absorption process using a wetted wall column, the fresh solvent enters from the top of the column (x=8 cm). CO_2 and H_2S mole fractions in the solvent increase in the flow direction with downward flow and absorption of acid gases in the solvent. Also, due to the reaction between CO_2 and DEA in the liquid phase, the mole fraction of reaction products increase as the liquid moves downward. Figure 18 shows the changes of CO_2 and H_2S mole fractions and Fig. 19 shows the changes of reaction products mole fractions in the liquid phase.

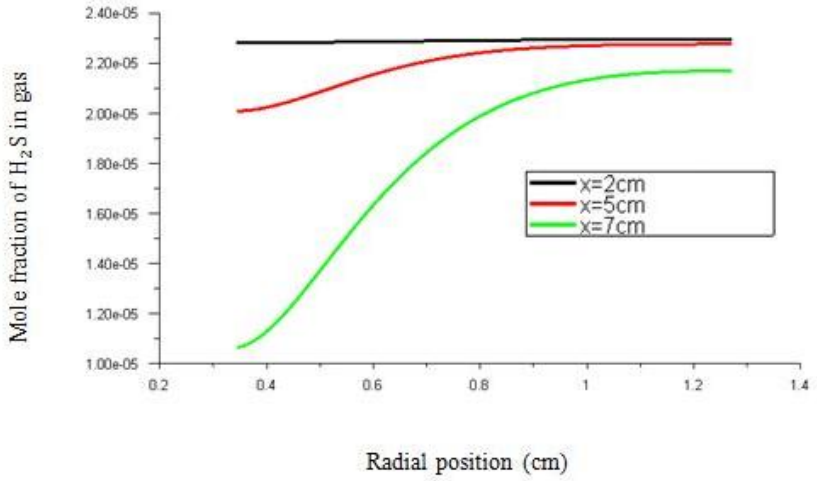

Figure 16. Comparison of H_2S mole fraction profiles in the gas phase at different sections of the column

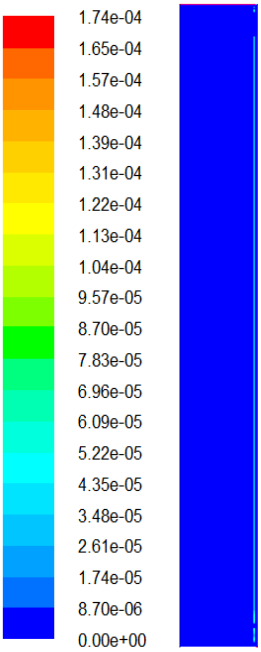

Figure 17. Reaction rate of CO_2 in the liquid phase in terms of ($kgmol/m^3.s$)

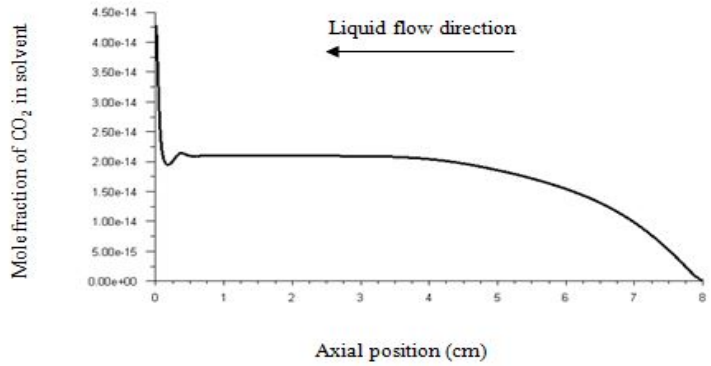

(a)

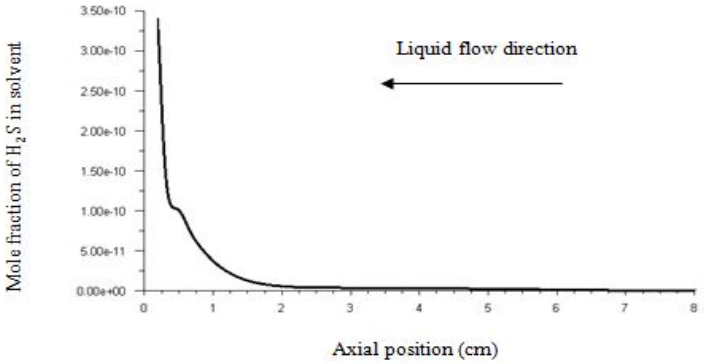

(b)

Figure 18. Changes in acid gases mole fractions in the solvent **(a)** CO_2 **(b)** H_2S

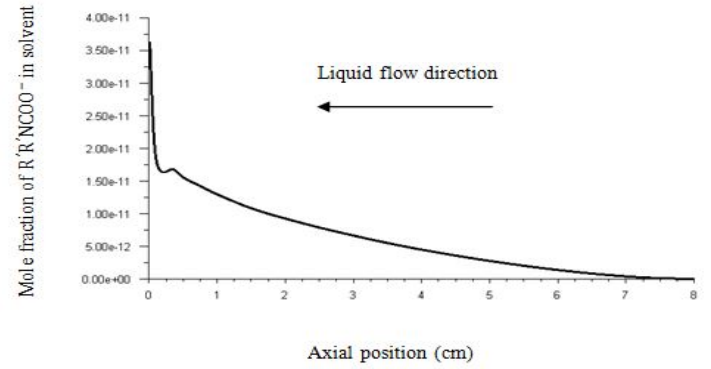

(a)

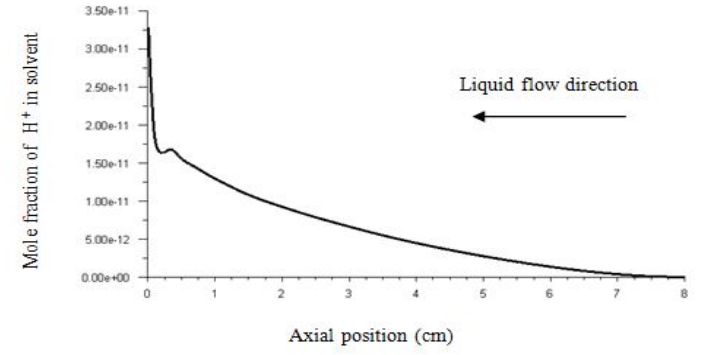

(b)

Figure 19. Changes of reaction products mole fractions in the solvent **(a)** $R'R'NCOO^-$ **(b)** H^+

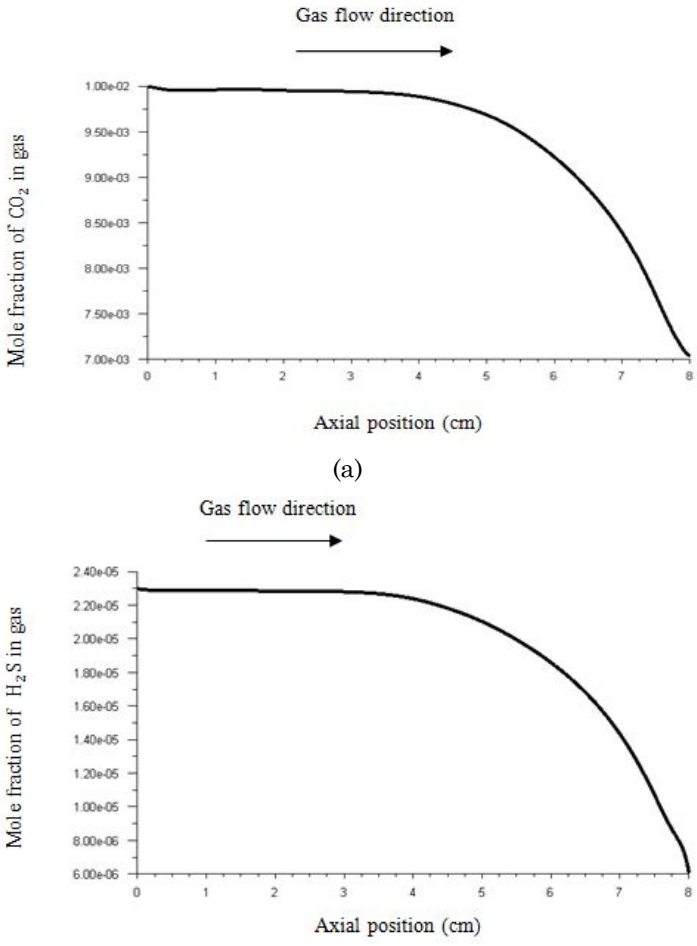

Figure 20. Changes in acid gases mole fractions in the gas phase **(a)** CO_2**(b)** H_2S

Table 5. The effect of temperature on absorption of CO_2 and H_2S in the solvent

Temperature (℃)	Mole fraction of CO_2 in output gas	Mole fraction of H_2S in output gas (ppm)
25	0.00701	6.04
30	0.00736	6.61
35	0.00741	7.39

The sour gas enters from the bottom of the column (x=0) and as it flows upward, acid components are absorbed in the solvent so that the output gas contains less CO_2 and H_2S. Figure 20 shows the changes of CO_2 and H_2S mole fractions in the gas phase.

3.5. The Effect of Temperature on the Absorption of Acid Gases

In order to evaluate the effect of temperature on the absorption of CO_2 and H_2S, the process was simulated at 25, 30 and 35℃. The results of CO_2 and H_2S mole fractions in the output gas are shown in Table 5. As can be seen, the mole fraction of acid gases increased with increasing temperature, which means the absorption amount is decreased as the temperature increased and this is completely explainable due to the exothermic absorption reaction.

4. Conclusions

The simultaneous absorption of carbon dioxide and hydrogen sulfide from natural gas into DEA solution in a wetted wall column was simulated using computational fluid dynamics (CFD). The volume of fluid (VOF) model was applied for simulating the gas-liquid two-phase flow. In order to study the hydrodynamics of the process, volume fraction distribution of the phases, liquid film formation and its thickness and velocity profiles were investigated and it was observed that the developed model was applicable to predict the liquid film thickness carefully in a wetted wall column and in

comparison with previous works there is no need to determine an initial value for liquid film thickness. Then by considering mass transfer from the gas phase to the liquid phase, absorption of CO_2 and H_2S into the solvent was simulated and concentration distribution of the components in the column was obtained. In order to study the effect of temperature on absorption of CO_2 and H_2S, the absorption process was simulated at 25, 30 and 35℃. It was observed that by increasing temperature, the absorption of acid gases was decreased. The simulation results were compared with the experimental data for output concentration of acid components in the gas and a good agreement was observed between them. In conclusion, the effects of different parameters on absorption process can be studied using these numerical simulations without the need for costly research experiments.

Acknowledgments

The authors acknowledge Sarkhoon & Qeshm gas treating company for providing us with the experimental data.

Note: This research did not receive any specific grant from funding agencies in the public, commercial, or not-for-profit sectors.

List of Symbols

A	Area (m^2)
a_e	Specific area ($\frac{m^2}{m^3}$)
C	Concentration ($\frac{kmol}{m^3}$)
D	Diffusion coefficient ($\frac{m^2}{s}$)
E	Enhancement factor
$\vec{F}$	Force (N)
$\vec{g}$	Gravity acceleration ($\frac{m}{s^2}$)
He	Henry's constant ($\frac{kPa.m^3}{kmol}$)
J	Diffusion flux ($\frac{kg}{m^2.s}$)
K	Interface curvature
k	Mass transfer coefficient ($\frac{m}{s}$)
L	Length (m)
$\dot{m}$	Mass flow rate ($\frac{kg}{s}$)
M	Molecular weight ($\frac{kg}{kmol}$)
$\hat{n}$	Unit normal vector
p	Pressure (Pa)
R_i	Production rate of component i in the chemical reaction ($\frac{kg}{m^3.s}$)
Re	Reynolds number
t	Time (s)
T	Temperature (k)
$\vec{v}$	Velocity vector ($\frac{m}{s}$)
x	Species mole fraction in liquid phase
y	Species mole fraction in gas phase
Y	Species mass fraction

Greek Symbols

α	Volume fraction
δ	Liquid film thickness (m)
μ	Viscosity ($\frac{kg}{m.s}$)
ρ	Density ($\frac{kg}{m^3}$)
σ	Surface tension ($\frac{N}{m}$)

Superscripts and Subscripts

g	Gas phase
i	interface
l	Liquid phase
m	amine solution
n	The nth component
w	Water

References

Abdulrahman, R. K., & Sebastine, I. M. (2013). Natural gas sweetening process simulation and optimization: A case study of Khurmala field in Iraqi Kurdistan region. *Journal of Natural Gas Science and Engineering,14*,116-120.

Baniadam, M., Fathikalajahi, J., & Rahimpour, M. R. (2009). Incorporation of Eulerian–Eulerian CFD framework in mathematical modeling of chemical absorption of acid gases into methyl diethanol amine on sieve trays. *Chemical Engineering Journal, 151*, 286-294.

Carey, T. R., Hermes, J. E., & Rochelle, G. T. (1991). A model of acid gas absorption/ stripping using methyldiethanolamine with added acid. *Gas Separation & Purification, 5*.

Chen, x., Closmann, F., & Rochelle, G. T. (2011). Accurate screening of amines by the Wetted Wall Column. *Energy Procedia, 4*, 101–108.

Fluent 6.3.26 users guide, fluent, Inc., (2006).

Haimour, N., & Sandall, O. C. (1983). Selective removal of hydrogen sulfide from gases containing hydrogen sulfide and carbon dioxide using diethanolamine. *Separation Science and Technology, 18*, 1221-1249.

Ho, C. D., Chang, H. C., Chen, H. J., Chang, C. L., Li, H. H., & Chang, Y. Y. (2011). CFD simulation of the two-phase flow for a falling film microreactor. *International Journal of Heat and Mass Transfer, 54*, 3740-3748.

Hosseini, S. M., Alizadeh, R., Fatehifar, E., & Alizadehdakhel, A. (2014). Simulation of gas absorption into string-of-beads liquid flow with chemical reaction. *Heat Mass Transfer, 50*, 1393-1403.

Hosseini, S. M. (2013). Simulation of fluid flow hydrodynamics in a wetted- wire column, M. Sc. Thesis, Sahand University of Technology, Tabriz, Iran.

Karlsson, H., & Svensson, H. (2017). Rate of absorption for CO_2 absorption systems using a wetted wall column. *Energy Procedia, 114*, 2009 – 2023.

Keshavarz, P., Fathikalajahi, J., & Ayatollahi, S. (2008). Mathematical modeling of the simultaneous absorption of carbon dioxide and hydrogen sulfide in a hollow fiber membrane contactor. *Separation and Purification Technology, 63*, 145-155.

Ko, J. J., Tsai, T. C., Lin, C. Y., Wang, H. M., & Li, M. H. (2001). Diffusivity of nitrous oxide in aqueous alkanolamine solutions. *J. Chem. Eng. Data, 46*, 160-165.

Lillia, S., Bonalumi, D., Fosbøl, P. L., Thomsen, K., & Valenti, G. (2018). Experimental data of the aqueous NH_3 and CO_2 absorption at temperatures from 15 °C to 35°C, NH_3 concentrations from 5% to 15% and CO_2 loadings from 0.2 to 0.6 measured with the Wetted Wall Column. *Datain Brief, 17*, 1240– 1244.

Mandal, B. P., & Bandyopadhyay, S. S. (2005). Simultaneous absorption of carbon dioxide and hydrogen sulfide into aqueous blends of 2-amino-2-methyl-1-propanol and diethanolamine. *Chemical Engineering Science, 60*, 6438-6451.

Mandal, B. P., & Bandyopadhyay, S. S. (2006). Simultaneous absorption of $CO_2$and H_2S into aqueous blends of N-methyldiethanolamine and diethanolamine. *Environ. Sci. Technol.,40*, 6076-6084.

Penttilä, A., Dell'Era, C., Uusi-Kyyny, P., & Alopaeus, V. (2011). The Henry's law constant of N_2O and CO_2 in aqueous binary and ternary amine solutions (MEA, DEA, DIPA, MDEA, and AMP). *Fluid Phase Equilibria, 311*, 59-66.

Rahimpour, M., Saidi, M., Baniadam, M., & Parhoudeh, M. (2013). Investigation of natural gas sweetening process in corrugated packed bed column using computational fluid dynamics (CFD) model. *Journal of Natural Gas Science and Engineering, 15*, 127-137.

Rezakazemi, M., Niazi, Z., Mirfendereski, M., Shirazian, S., Mohammadi, T., & Pak, A. (2011). CFD simulation of natural gas sweetening in a gas–liquid hollow-fiber membrane contactor. *Chemical Engineering Journal, 168*, 1217-1226.

Rodriguez-Flores, H. A., Mello, L. C., Salvagnini, W. M., & de Paiva, J. L. (2013). Absorption of CO_2 into aqueous solutions of MEA and AMP in a wetted wall column with film promoter. *Chemical Engineering and Processing, 73*, 1– 6.

Taheri, M., Mohebbi, A., Hashemipour, H., & Rashidi, A. M. (2016).Prepration of graphene-amine nanofluid for absorption of carbon dioxide (CO_2) and hydrogen sulfide (H_2S) from natural gas stream in a wetted wall column. *Gas Processing Journal,4(1), 29-41*.

Taheri, M., Mohebbi, A., Hashemipour, H., & Rashidi, A. M. (2016). Simultaneous absorption of carbon dioxide (CO_2) and hydrogen sulfide (H_2S) from CO_2-H_2S -CH_4 gas mixture using amine-based nanofluids in a wetted wall column. *Journal of Natural Gas Science and Engineering, 28*,410- 417.

Versteeg, G. F., Van Dijck, L. A. J., & Van Swaaij, W. P. M. (1996). On the kinetics between CO2 and alkanolamines both in aqueous and non-aqueous solutions. and overview. *Chem. Eng. Comm., 144*, 113-158.

Wang, C., Xu, Z., Lai, C., & Sun, X. (2018). Beyond the Standard Two-Film Theory: Computational Fluid Dynamics Simulations for Carbon Dioxide Capture in a Wetted Wall Column. *Chemical EngineeringScience, 184*, 103-110.

Xu, Y. Y., Paschke, S., Repke, J. U., Yuan, J. Q., & Wozny, G. (2009). Computational approach to characterize the mass transfer between counter-current gas-liquid flow. *Chem. Eng. Technol., 32*, 1227-1235.

Yih, S. M., & Hsu, T. Y. (1985). Gas absorption into wavy and turbulent non-Newtonian falling liquid films in a wetted-wall column. *Chemical Engineering Communication, 34*, 65-76.

Yih, S. M., & Sun, C. C. (1987). Simultaneous absorption of hydrogen sulphide and carbon dioxide into potassium carbonate solution with or without amine promoters. *The Chemical Engineering Journal, 34*, 65-72.

Zhou, D. W., Gambaryan-Roisman, T., & Stephan, P. (2009). Measurement of water falling film thickness to flat plate using confocal chromatic sensoring technique. *Experimental Thermal and Fluid Science, 33*, 273–283.